International Journal of Thermophysics, Vol. 17, No. 1, 1996

Silica Under Very Large Positive and Negative Pressures: Molecular Dynamics Simulations on Parallel Computers[1]

P. Vashishta,[2,3] R. K. Kalia,[2] A. Nakano,[2] and W. Jin[2]

A highly efficient multiresolution algorithm has been developed to carry out large-scale molecular dynamics (MD) simulations for systems with long-range Coulomb and three-body covalent interactions. The algorithm combines the reduced cell and fast multipole methods and multiple time-step approach. Pressure-induced structural transformation, loss of intermediate range order, and dynamical correlations in SiO_2 glass are investigated with the molecular-dynamics method. At twice the normal density, the Si–O bond length increases, the Si–O coordination changes from 4 to 6, and the O–Si–O band-angle changes from 109 to 90°. This is a tetrahedral-to-octahedral transformation, which was reported by Meade, Hemley, and Mao. Results for phonon density of states also reveal significant changes at high pressures. The multiresolution MD approach has been used to investigate the structural properties and mechanical failure in microporous silica. Structural correlations are characterized by the fractal dimension, internal surface area, and pore surface-to-volume ratio. Critical behavior at fracture is analyzed in terms of pore percolation, and kinetic roughening of fractured surface is also investigated.

KEY WORDS: densified silica; fast multipole method; fracture; high pressure; intermediate range order; kinetic roughening; molecular dynamics; multiresolution algorithms; parallel computing; porous silica; structural transformations.

1. INTRODUCTION

We have designed a variety of algorithms to implement molecular dynamics (MD) simulations on emerging parallel architectures [1–3]. For

[1] Paper presented at the Twelfth Symposium on Thermophysical Properties, June 19–24, 1994, Boulder, Colorado, U.S.A.

[2] Concurrent Computing Laboratory for Materials Simulations, Department of Physics and Astronomy, and Department of Computer Science, Louisiana State University, Baton Rouge, Louisiana 70803-4001, U.S.A.

[3] To whom correspondence should be addressed.

840/17/1-13

systems with finite-range interactions, a domain–decomposition algorithm is used to implement the multiple-time step (MTS) approach to MD simulations on distributed-memory MIMD (multiple instruction multiple data) machines. Parallel algorithms are also designed for MD simulations of bulk Coulombic systems. The performances of these algorithms are tested on the Intel Touchstone Delta and IBM SP1 architectures. The computational complexities of these algorithms are O(N) and parallel efficiencies close to 0.9.

Recently Meade, Hemley, and Mao have carried out *in situ* high-pressure (8-to 42-GPa) X-ray diffraction experiments on SiO_2 glass [4]. These measurements reveal significant changes in the short-range and intermediate-range order (IRO). MD simulations are used to investigate the structural transformation, loss of intermediate-range order, and dynamical behavior of SiO_2 glass at high pressures [5].

Porous silica has numerous technological applications [6]. Since these applications are due to the remarkable porous structure of the system, it is important to understand the size and spatial distributions of pores [7, 8] and the morphology of pore interfaces [9]. Simulations of porous silica, in the density range 2.2–0.1 $g \cdot cm^{-3}$, are carried out on 41,472- and 1,119,744-particle systems using MIMD computers.

2. MULTIRESOLUTION MD ALGORITHM

Realistic modeling of materials relies on high-quality interatomic potentials. They must include the effects of the long-range Coulomb interaction, charge-dipole interaction, steric hindrance, and covalent bonding [10]. The use of these potentials for large systems requires enormous computing resources. The most prohibitive factor for large-scale MD simulations is the long-range Coulomb potential. The evaluation of the Coulomb potential for an N-particle system requires $O(N^2)$ operations, which makes large-scale MD simulations difficult.

The development of hierarchical algorithms has resolved this difficulty. The fast multipole method (FMM) employs truncated multipole expansions for the potential field, and calculates the Coulomb potential with O(N) operations [11]. In the FMM, a hierarchy of cells is defined by dividing the total system into smaller cells. To achieve a consistent accuracy, farther cells are combined to form a larger cluster of cells, and multipoles are calculated for those clusters at lower levels of the hierarchy (see Fig. 1b). For many simulations in materials science, the summation over repeated images of the original system needs to be performed to minimize surface effects. Recently the reduced-cell multipole method (RCMM) has been developed to carry out the infinite summation most efficiently [2,

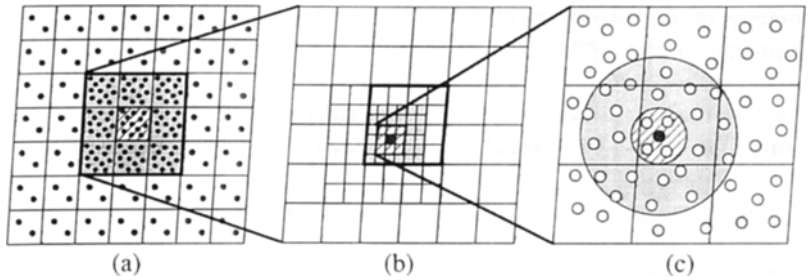

Fig. 1. Multiresolution in space. (a) Periodically repeated images of the original MD box. Replacing far images by a small number of particles with the same multipole expansion up to a certain order reduces the computation enormously while maintaining the necessary accuracy. (b) A hierarchy of cells used in the fast multipole method. (c) The near-field force on a particle is due to primary, secondary, and tertiary neighbor particles.

12]. Distant images each including multimillion particles can be replaced, without loss of accuracy, by a few tens of particles which have the same leading multipoles as the original system. The Edwald summation is carried out for these reduced images with little computation effort (see Fig. 1a).

Another computational difficulty arises from the non-Coulombic part of the potential. For a realistic description of materials, the potential in the medium range (below $r_c \sim 5$–10 Å) involves complicated non-Coulombic terms. In the FMM, the smallest cell of the hierarchy must be larger than r_c. Accordingly, forces from thousands of other atoms in the 27 nearest-neighbor cells must be calculated directly, resulting in enormous computing.

We employ the multiple-time step (MTS) approach [2, 13] to reduce the computation over the medium range of length scales. Contrary to the above cell-based methods, this method is adaptive since it uses neighbor lists and different time steps are employed for different spatial ranges (see Fig. 1c). The MTS algorithm typically speeds up a calculation by a factor of 5 to 7.

Three-body potentials are necessary to represent covalent interactions. We employ a separable, tensor decomposition scheme to speed up the calculation of three-body forces by a factor of two [2, 14].

We use the domain decomposition approach to implement the multiresolution MD (MRMD) algorithm on parallel architectures. On a parallel computer with p procesors, the simulation system is divided into p subsystems of equal volume, and each physical subsystem is assigned to a processor. To calculate the intermediate-range forces, information about the particles in the skin layers must be communicated among the processors. The MTS approach reduces the volume of these messages significantly by

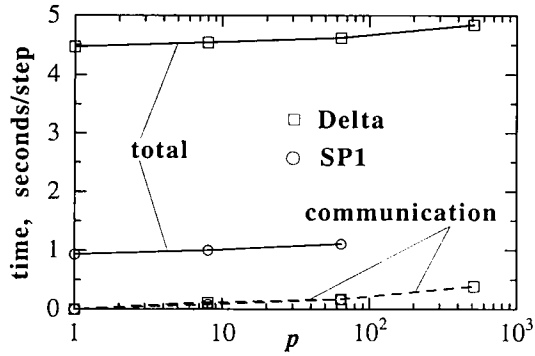

Fig. 2. Execution time (solid curves) and communication time (dashed) per MD time step for SiO_2. Circles and squares represent the results on the IBM SP1 and Intel Touchstone Delta, respectively. Here p is the number of nodes. The size of the system, N, increases at $8232\,p$.

skipping the message passing associated with the secondary and tertiary neighbors.

The performance of the multiresolution algorithm is tested for variable-shape MD simulations [15] of the SiO_2 system on the 512-node Intel Touchstone Delta machine at Caltech and the 128-node IBM SP1 system at Argonne National Laboratory. Figure 2 shows the execution time per MD step as a function of the number of processors, p. The number of particles is taken to be $8{,}232\,p$. For a 4.2 million-particle system, the program requires only 4.84 s per MD step on the 512-node Delta. Communication accounts for only 8% of the total elapsed time. On the IBM SP1, the computation part runs 4.8 times faster than on the Delta, while the communication performs at about the same speed. As a result, the communication overhead is slightly larger on the SP1 [2].

3. MD SIMULATION OF SILICA AT HIGH PRESSURES

Recently Meade et al. [4] have carried out *in situ* high-pressure (8- to 42-GPa) X-ray diffraction experiments on SiO_2 glass. These measurements reveal significant changes in the short-range and intermediate-range order (IRO). The position of the first sharp diffraction peak (FSDP) in X-ray structure factor, the fingerprint of IRO, changes from 1.55 $Å^{-1}$ at 8 GPa to 2.37 $Å^{-1}$ at 42 GPa. At the same time, there is a significant decrease in the height and increase in the width of the FSDP. Furthermore, the pair correlation function shows that the nearest-neighbor (nn) tetrahedral coordination of Si–O changes to octahedral coordination as the pressure is

increased from 8 to 42 GPa. Raman and infrared spectra at pressures greater than 28 GPa reveal the absence of tetrahedral vibrational modes [16, 17].

Molecular-dynamics simulations were performed with interatomic potentials comprising two- and three-body terms [10]. The MD simulations were carried out at normal mass density $\rho_0 = 2.20\ \mathrm{g \cdot cm^{-3}}$, and at pressures 0.9, 5.4, 22.7, and 42.3 GPa, corresponding to densities $\rho = 2.64$, 2.94, 3.53, and 4.28 $\mathrm{g \cdot cm^{-3}}$, respectively.

The SiO_2 glasses were generated by quenching well-equilibrated liquids at high temperatures (~ 4000 K) [10]. At each temperature and

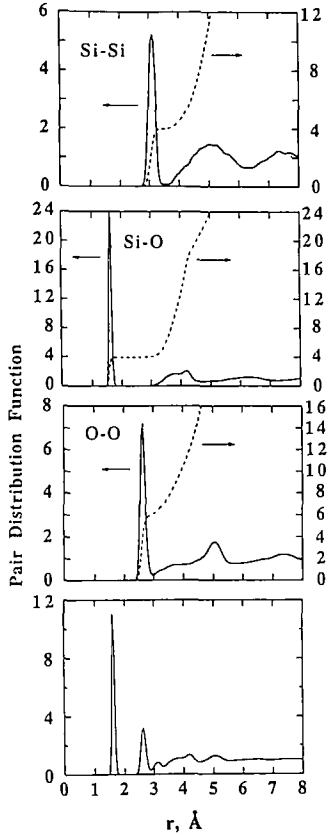

Fig. 3. MD partial pair-distribution functions (solid lines) and coordination numbers (dashed lines) for SiO_2 glasses at normal density at 300 K.

density, structural and dynamical correlations were calculated with MD trajectories of at least 30 ps.

In the normal-density MD glass, the FSDP is located at 1.6 $Å^{-1}$. With an increase in the density, the height of the FSDP decreases, its width increases, and its position shifts to higher values of q. Note that simple elastic compression [i.e., $(\rho/\rho_0)^{1/3}$] cannot account for the observed shift in the position of the FSDP. Elastic compression corresponding to density

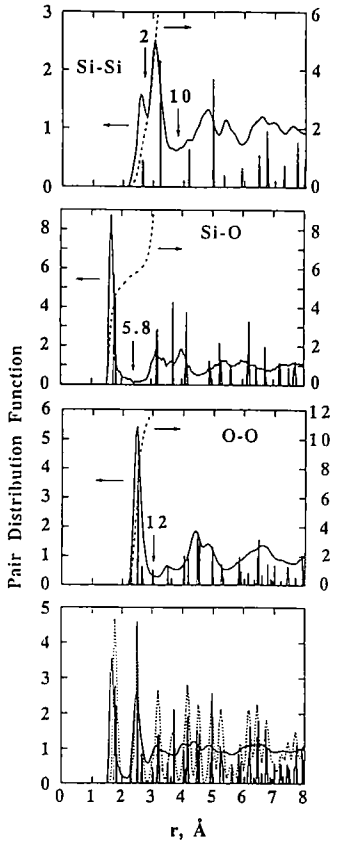

Fig. 4. MD partial pair-distribution functions (solid lines) and coordination numbers (dashed lines) for SiO_2 glasses at stishovite density at 300 K. Sharp peaks in the figure at $4.28\,g \cdot cm^{-3}$ correspond to pair-distribution functions for crystalline stishovite.

increases of 20, 33, 60 and 95% would shift the FSDP to 1.71, 1.77, 1.88, and 2.01 $Å^{-1}$, whereas the simulation results reveal higher values for the position of the FSDP: 1.85, 1.94, 2.15, and 2.19 $Å^{-1}$. The high pressure X-ray measurements by Meade, Hemley, and Mao [4] reveal similar behavior for the FSDP.

Partial pair-distribution functions, $g_{ab}(r)$, at the normal and the highest density are shown in Figs. 3 and 4. The position of the first peak in $g_{Si\text{-}O}(r)$ and the corresponding Si–O coordination remain unchanged up to 3.53 $g \cdot cm^{-3}$. At a pressure of 42.3 GPa, where the glass density (4.28 $g \cdot cm^{-3}$) reaches the stishovite density, the first peak in $g_{Si\text{-}O}(r)$ occurs at 1.67 instead of 1.61 Å and the Si–O coordination increases from 4 to 5.8. In stishovite, the highest-density crystalline phase of SiO_2, Si–O bond lengths are 1.76 and 1.81 Å and the Si–O coordination is 6. In the glass at 4.28 $g \cdot cm^{-3}$, the second peak in $g_{Si\text{-}O}(r)$ is at 3.15 Å, close to the next-nearest-neighbor (nnn) Si–O distance ($\sim$3.20 Å) in the stishovite [5].

Figures 3 and 4 also show how the Si–Si pair-distribution function changes upon densification. The first peak splits into two peaks when the density increases to 4.28 $g \cdot cm^{-3}$. One of these peaks is located at 2.59 Å, close to the nn Si–Si distance (2.67 Å) in the stishovite. The second peak appears at 3.07 Å, which is close to the nnn Si–Si distance (3.24 Å) in the stishovite. The area under the first peak gives a coordination of 2, while the area under the first two peaks is 10. At normal density, the nn O–O coordination is 6. It increases to 10 at 3.53 $g \cdot cm^{-3}$ and to 12 at 4.28 $g \cdot cm^{-3}$. In Stishovite, the O–O coordination is 12.

At normal density, the O–Si–O bond angle distribution has a peak at 109°, with a full width at half maximum (FWHM) of 10°. There is a dramatic change in the distribution when the glass density reaches the stishovite density: the O–Si–O distribution has broad peaks at 90 and 171°. On the other hand, in the crystalline stishovite, the O–Si–O angles are 81.35, 90, 98.65, and 180°. In the normal-density SiO_2 glass, the Si–O–Si bond-angle distribution has a peak at 142° and the FWHM of this peak is 26° [10, 18]. At the stishovite density, the Si–O–Si bond angle in the glass has broad peaks around 95 and 128°. These values are close to the Si–O–Si angles, 98.65 and 130.67°, in the stishovite crystal. Thus, the results for pair-distribution functions and bond-angle distributions at 4.28 $g \cdot cm^{-3}$ contain strong evidence for distorted $Si(O_{1/3})_6$ octahedra in the glass, joined at corners and sharing edges as well.

4. MD SIMULATION OF POROUS SILICA

From the technological standpoint, it is important to know the size distribution, the internal surface area and surface-to-volume ratio, and the

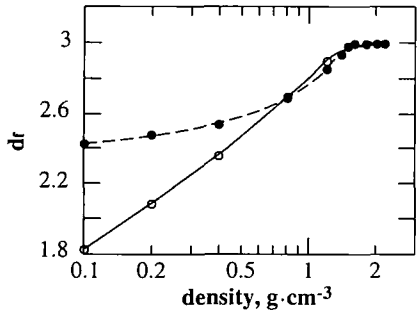

Fig. 5. MD results on fractal dimension as a function of density. Open circles are for MD configurations prepared at temperature 300 K, while filled circles are for 1000 K.

interface texture of pores in porous glasses. MD simulations were performed to determine these structural parameters over a wide range of densities, from 2.2 to as low as 0.1 $g \cdot cm^{-3}$ [7, 8]. The MD simulations reveal a structural transition from the condensed amorphous phase to a low-density porous phase. The latter is a fractal network whose dimensionality decreases rapidly with a decrease in the density. Figure 5 shows the fractal dimension as a function of the density.

Recent experiments on a wide variety of materials reveal that fracture surfaces exhibit scaling properties. The root-mean-square surface fluctuations averaged over a distance l obey the scaling relation, $W \sim l^{\alpha}$. The roughness exponent, α, of cracks in a variety of brittle materials has been found to be close to 0.87 [9]. This has led to the suggestion that the roughness exponent for fracture surfaces has a universal value. However, the universality of the roughness exponent on the nanometer scale is still an unresolved issue.

We have performed large-scale MD calculations on amorphous silica, investigating the growth of pores with a decrease in the density of the system. At a critical density, some pores percolate through the entire system by catastrophic growth.

We analyze the interface roughness of a percolating pore by defining a two-dimensional height function, $h(x, y)$, for the pore. The height–height correlation function, $g(\sigma)$, is defined as

$$g(\sigma) = \langle [h(x + x_0, y + y_0) - h(x_0, y_0)]^2 \rangle^{1/2} \tag{1}$$

where $\sigma = (x^2 + y^2)^{1/2}$. The function scales as $g(\sigma) \propto \sigma^{\alpha}$. The exponent α is found to be 0.87 ± 0.01 (see Fig. 6). This is in excellent agreement with

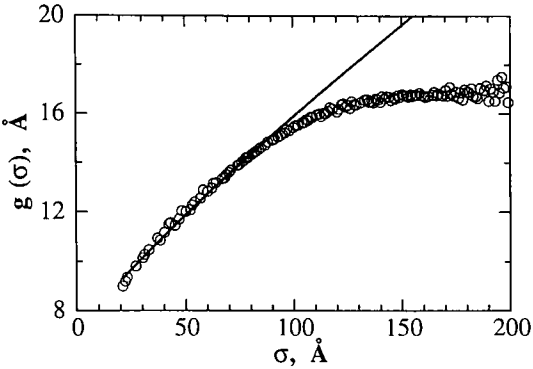

Fig. 6. The height–height correlation function of a percolating pore at a mass density of $1.4\,g \cdot cm^{-3}$. The open circles are the MD results and the solid curve represents $g(\sigma) \propto \sigma^{\alpha}$.

experimental measurements on mesoscopic and macroscopic length scales. These MD results support the conjectured universality of the roughness exponent even on the nanometer scale [19].

ACKNOWLEDGMENT

This work was supported by the U.S. Department of Energy, Office of Energy Research, Basic Energy Science, Materials Science Division, Grant DE-FG05-92ER45477.

REFERENCES

1. R. K. Kalia, S. W. de Leeuw, A. Nakano, and P. Vashista, *Comput. Phys. Commun.* **74**: 316 (1993).
2. A. Nakano, P. Vashishta, and R. K. Kalia, *Comput. Phys. Commun.* **77**:303 (1993); A. Nakano, R. K. Kalia, and P. Vashishta, *Comput. Phys. Commun* (in press).
3. P. Vashishta, R. K. Kalia, S. W. de Leeuw, D. L. Greenwell, A. Nakano, W. Jin, J. Yu, L. Bi, and W. Li, *Comp. Mat. Sci.* **2**:180 (1994).
4. C. Meade, R. J. Hemley, and H. K. Mao, *Phys. Rev. Lett.* **69**:1387 (1992).
5. W. Jin, R. K. Kalia. P. Vashishta, and J. P. Rino, *Phys. Rev. Lett.* **71**:3146 (1993); W. Jin, R. K. Kalia, P. Vashishta, and J. P. Rino, *Phys. Rev. B* (in press).
6. J. Fricke, *J. Non-Cryst. Solids* **121**:188 (1990).
7. J. Kieffer and C. A. Angell, *J. Non-Cryst. Solids* **106**:336 (1988).
8. A. Nakano, L. Bi, R. K. Kalia, and P. Vashishta, *Phys. Rev. Lett.* **71**:85 (1993).
9. K. J. Måløy, A Hansen, E. L. Hinrichsen, and S. Roux, *Phys. Rev. Lett.* **68**:213 (1992).
10. P. Vashishta, R. K. Kalia, J. P. Rino, and I. Ebbsjö, *Phys. Rev. B* **41**:12197 (1990).
11. L. Greengard and V. Rokhlin, *J. Comput. Phys.* **73**:325 (1987).
12. H.-Q. Ding, N. Karasawa, and W. A. Goddard, *Chem. Phys. Lett.* **196**:6 (1992).
13. W. B. Streett, D. J. Tildesley, and G. Saville, *Mol. Phys.* **35**:639 (1978).

14. D. Frenkel, in *Simple Molecular Systems at Very High Density*, A. Polian, P. Loubeyre, and N. Boccara, eds. (Plenum, New York, 1989), p. 411.
15. M. Parrinello and A. Rahman, *J. Appl. Phys.* **52**:7182 (1981).
16. R. J. Hemley, H. K. Mao, P. M. Bell, and B. O. Mysen, *Phys. Rev. Lett.* **57**:747 (1986).
17. Q. Williams and R. Jeanloz, *Science* **239**:902 (1988).
18. R. Dupree and R. F. Pettifer, *Nature* **308**:523 (1984).
19. A. Nakano, R. K. Kalia, and P. Vashishta, *Phys. Rev. Lett.* **73**:2336 (1994).